Research Article

Hybrid TiO_2/WO_3 nanoparticles fabricated via a sol–gel process using amphiphilic poly(ε-caprolactone)-*block*-poly(acrylic acid) diblock copolymer as template and their high visible light photocatalytic activity

Tingting Xu[1,2] · Haotian Wu[1] · Kun Cui[1] · Qiaoling Zhao[1] · Jin Huang[1] · Liuhe Wei[2] · Zhi Ma[1]

Abstract

The hybrid TiO_2/WO_3 nanoparticles with different doping ratios of tungsten were synthesized from titanium tetra-isopropoxide and tungsten hexachloride (WCl_6) as precursors via a sol–gel process using poly(ε-caprolactone)-*b*-poly(acrylic acid) (PCL-*b*-PAA) diblock copolymer as a template. The morphology, crystal structure, chemical and physical property of the fabricated TiO_2/WO_3 nanoparticles were characterized by scanning electron microscopy, transmission electron microscopy, powder X-ray diffraction, X-ray photoelectron spectroscopy and so on. N_2 adsorption–desorption analysis revealed that the surface area (40.6 $m^2\ g^{-1}$), pore volume (0.11 $cm^3\ g^{-1}$) and average pore size (8.56 nm) of such TiO_2/WO_3 nanoparticles. The resulting hybrid TiO_2/WO_3 nanoparticles (average diameter: ca. 100–200 nm) with proper doping ratio of tungsten exhibited the enhanced photocatalytic activity than that of the commercial P25 in the degradation of methylene blue.

Graphic Abstract

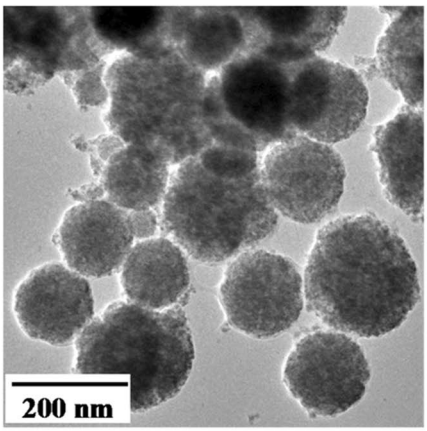

TEM image of hybrid TiO_2/WO_3 precursor nanoparticles (Ti:W=85:15) after acetone extraction several times.

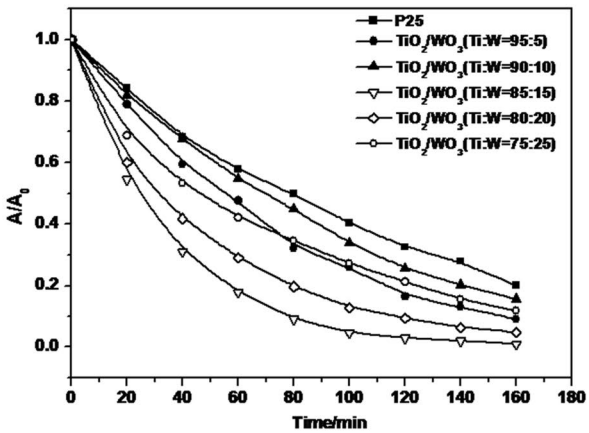

Photodegradation curves of methylene blue catalyzed by hybrid TiO_2/WO_3 nanoparticles with different Ti/W ratios and P25.

Keywords Hybrid TiO_2/WO_3 nanoparticles · Sol–gel process · Template · Block copolymer · Photocatalysis

✉ Liuhe Wei, weiliuhe@zzu.edu.cn; ✉ Zhi Ma, mazhi728@sioc.ac.cn | [1]Key Laboratory of Synthetic and Self-Assembly Chemistry for Organic Functional Molecules, Center for Excellence in Molecular Synthesis, Shanghai Institute of Organic Chemistry, Chinese Academy of Sciences, 345 Lingling Road, Shanghai 200032, People's Republic of China. [2]Zhengzhou Key Laboratory of Elastic Sealing Materials, College of Chemistry and Molecular Engineering, Zhengzhou University, Zhengzhou 450002, People's Republic of China.

SN Applied Sciences (2019) 1:866 | https://doi.org/10.1007/s42452-019-0718-7

Received: 7 May 2019 / Accepted: 4 June 2019 / Published online: 17 July 2019

1 Introduction

Amphiphilic diblock copolymer is formed by the junction of covalent bond between one hydrophilic polymer segment and the other hydrophobic polymer segment, which can form micelles or aggregates by self-assembly in selective solvent because of the thermodynamic incompatibility between two different polymer segments and phase separation characteristics. Therefore, it can form micron- or nano-scale micro-reactor in solution with controllable size by regulating the length and property of polymer segments [1]. Meanwhile, different shapes of micro-reactor such as ball, rod and vermicular, etc. can be obtained by changing the solvent composition, pH, temperature during the amphiphilic diblock copolymer's self-assembly [2, 3].

Poly(ε-caprolactone) (PCL) is a kind of semicrystalline polymer with good biocompatibility, biodegradability and etc. [4]. In recent years, the polymer self-assembly technology has received considerable attention, and the amphiphilic diblock copolymer prepared from hydrophobic polycaprolactone and hydrophilic polymer is the focus of attention. Poly(acrylic acid) (PAA) is a pH sensitive weak electrolyte, it can unite with nonionic polymers electron acceptor and cationic polyelectrolyte, and interact with cations [5]. Therefore, the synthesis of amphiphilic copolymer contains PCL and PAA blocks make great significance, since it can not only improve the such polymer's performance, but also expand the its application [6].

With the continuous development of nanotechnology, multifunctional nanocomposite draws more and more attention, especially that based on block copolymer templates [7]. The preparation of nanometer materials was optimized because of the block copolymers' properties. Several synthetic methodologies have been widely developed to prepare TiO_2 material with significant properties, such as sol–gel method [8–11], micelle and inverse micelle methods [12–14], sol method [15, 16], hydrothermal method [17–21], evaporation-induced self-assembly method [21], solvo-thermal method [22, 23], chemical vapor deposition [24], physical vapor deposition [25], direct oxidation method [26], and so on. The sol–gel process is one of the most widely used methodology for preparing nanoparticles due to several advantages, such as high purity, good uniformity, low processing temperature, stability and versatility of processing [27, 28]. And the sol–gel process with diblock copolymer as template has been applied in the preparation of thin film, ceramic fiber materials, microporous inorganic membrane, porous aerogel material and functional composite [29, 30]. Nanometer TiO_2 has became one of research hotspots in the field of material due to its significant physical and chemical properties. It has good stability, high catalytic efficiency, no secondary pollution, non-toxic and low cost as photocatalyst, and has special advantages in the degradation of toxic and refractory organic matter and inorganic matter. TiO_2 photocatalysis material has practical application in many areas, such as the self-cleaning materials, air purification, wastewater treatment, super hydrophilic coating, etc. [31].

While, with the exponential growth of research activities, modified doping have been widely progressed, such as nonmetallic doping [32–38], metallic doping [39–42] and semiconductor doping [43–47]. Among the variety of methods targeting improve the photocatalytic activities, the semiconductor doping attracted much attention. Since the semiconductor of different width forbidden band compounded with each other, urging the separation of electronic-hole, reducing electronic restructuring, widen the range of spectral response, further improve the photocatalytic efficiency in consequence. Carcel et al. [43] reported the photodegradation for methyl orange (MO) of TiO_2, WO_3 and TiO_2/WO_3 films in different pH, and get films of improved photocatalytic efficiency with the addition of H_2O_2. Yang et al. [44] obtained composite that shows higher acetaldehyde degradation efficiency than mono-TiO_2 in the presence of WO_3, and studied the effect on the different ratio of W/Ti compounds on the degradation efficiency. Ren et al. [45] reported TiO_2–SiO_2 catalyst that prepared using $TiOSO_4{\cdot}2H_2O$ and SiO_2 as precursor, and show fine catalysis activity after calcinations. Fateh et al. [46] obtained TiO_2–SiO_2 films via dip-coating method on polycarbonate resin template showing improved photocatalytic efficiency after the combination of SiO_2.

Herein, we report the synthesis of hybrid TiO_2/WO_3 nanoparticles via a sol–gel process by self-assembly amphiphilic diblock copolymer PCL-*b*-PAA as the template, toluene as solvent, using titanium tetra-isopropoxide (TTIP) and tungsten hexachloride (WCl_6) as precursor. Transmission electron microscopy (TEM), scanning electron microscope (SEM), X-ray diffraction analyzer (XRD), X-ray photoelectron spectroscopy analyzer (XPS), UV–Visible spectroscopy (UV–vis), thermal gravity analysis (TGA), etc. had been used to characterize the morphology, structure and performance of hybrid TiO_2/WO_3 nanoparticles. The effects of different doping ratios on photocatalytic performance of TiO_2/WO_3 nanoparticles were investigated in terms of degradation of methylene blue (MB).

2 Experimental

2.1 Chemicals and materials

The amphiphilic diblock copolymer, poly(ε-caprolactone)-*block*-poly(acrylic acid) (PCL-*b*-PAA) [$M_w/M_n = 1.18$; M_n (PCL) = 8600 g mol^{-1}; M_n (PAA) = 4200 g mol^{-1}] prepared in a similar procedure reported in our previous work [6], acted as a template in sol–gel process. Toluene was refluxed over sodium and distilled under a nitrogen atmosphere before use. Concentrated hydrochloric acid (HCl, 37%) and methylene blue (MB) were purchased from Sinopharm Chemical Reagent Co. Ltd. Titanium tetra-isopropoxide (TTIP) and tungsten hexachloride (WCl_6) were purchased from Aladdin Chemistry Co. Ltd.

2.2 Preparation of hybrid TiO_2/WO_3 nanospheres

All manipulations involving low moisture conditions were carried out using Schlenk techniques. In a typical preparation, 200 mg dried PCL-*b*-PAA was dissolved in 12 mL toluene under nitrogen atmosphere in a Schlenk tube with a magnetic stir bar. Then, 1 mL WCl_6 solution in toluene (0.1 g mL^{-1}) was injected into the reaction system. The solution was stirred for 1 h at room temperature. After that 0.4 mL TTIP was added to the solution and stirred for 2 h. Then, 0.1 mL HCl (37%) was added into the solution. The mixture was stirred for 2 h and aged for 24 h at room temperature. The different molar ratio of TTIP and WCl_6 in Ti:W = 95:5, 90:10, 85:15, 80:20 and 75:25 were employed respectively. After that the sample was annealed at 100 °C for 1 h followed by calcination at 500 °C, 600 °C or 700 °C for 5 h.

To obtain the TiO_2/WO_3 precursor nanoparticles for TEM observation, the mixed precursor solution in the Schlenk tube was extracted by acetone several times to remove the polymer residue. The mixture was then added into 30 mL acetone and stirred for 30 min. After centrifuging the solution, the supernatant was removed by a dropper. This process was repeated 5 times. A suspension of TiO_2/WO_3 precursor nanoparticles was obtained and observed by TEM.

2.3 Instruments and measurements

The as-synthesized TiO_2/WO_3 nanoparticles before and after calcinations were characterized by SEM (JSM-6390LV, JEOL Ltd.), TEM (JEM-1400, 120 kV, JEOL Ltd.), powder X-ray diffraction (XRD) (Cu-Kα radiation (λ = 1.5418 Å), X'pert PRO, Panalytical Co.) and X-ray photoelectron spectroscopy (XPS) (Al-Kα radiation (hν = 1486.6 eV), Thermo ESCALAB 250Xi, USA). The UV–Visible absorption spectra were recorded with a UNICO UV-2102PC spectrophotometer. Nitrogen adsorption–desorption isotherms of TiO_2/WO_3 nanoparticles were measured by Micromeritics ASAP 2020 surface area and porosity analyser. The photocurrent measurements of TiO_2/WO_3 spin-coated film were carried out with a CHI 660C workstation. The photoluminescence (PL) analyses were measured at room temperature by a Fluorolog-3-P UV–VIS-NIR fluorescence spectrophotometer illuminated with a 360 nm He–Cd laser.

2.4 Photocatalytic activities

The photocatalytic activity of the hybrid TiO_2/WO_3 nanoparticles was tested under visible light. A 400 W high-pressure mercury lamp was placed 10 cm away from the reaction vessel, which was used to provide a full-spectrum emission without any filter to simulate the sunlight source. The illumination intensity was 5 W m^{-2}. The photocatalytic activities of TiO_2/WO_3 nanoparticles were evaluated by photodegradation of MB. The selected photocatalyst was dispersed in the MB solution (10 mg mL^{-1}) to achieve a concentration of 1 mg mL^{-1}. The mixed suspension was first stirred in the dark for 1 h to reach the adsorption–desorption equilibrium of MB. The concentration of residual MB was determined by recording the decrease in the maximum absorbance of MB at 654 nm after various reaction times using UV–vis spectrophotometer every 20 min.

3 Results and discussion

TiO_2/WO_3 precursor nanoparticles were formed inside the PCL-*b*-PAA micelles with PCL segment as "shell" and the PAA segment as "core" [45] which coordinated with WCl_6 and TTIP. Although extracted by acetone several times, TiO_2/WO_3 precursors particles with irregular morphology were still formed (Fig. 1a). However, spherical nanoparticles of TiO_2/WO_3 could be formed (Fig. 1b) after acetone extraction followed by calcinations at 600 °C for 5 h.

TEM observation (Fig. 2) showed that TiO_2/WO_3 precursor after acetone extraction several times appeared as regular spheres with diameter size from 100 to 200 nm. Such spherical morphology indicated that the hydrolysis of TTIP and WCl_6 happened in the core of the PCL-*b*-PAA micelles as templating agent. The effects of the molar ratio of PCL/PAA segment, the molar ratio of TTIP/WCl_6/PAA and etc. on the morphology and property of the obtained TiO_2/WO_3 nanoparticles are under investigation.

Energy dispersive spectroscopy (EDS) analysis was conducted to confirm the composition of the hybrid TiO_2/WO_3 nanoparticles as shown in Fig. 3. The characteristic peaks of Ti, W, O and C atoms can be clearly

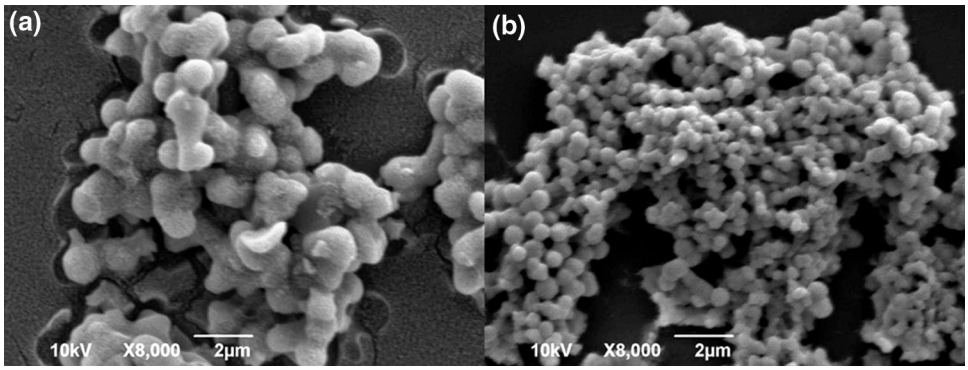

Fig. 1 SEM images of hybrid TiO_2/WO_3 nanoparticles (Ti:W = 85:15): **a** after acetone extraction without calcination; **b** after acetone extraction and calcination at 600 °C for 5 h

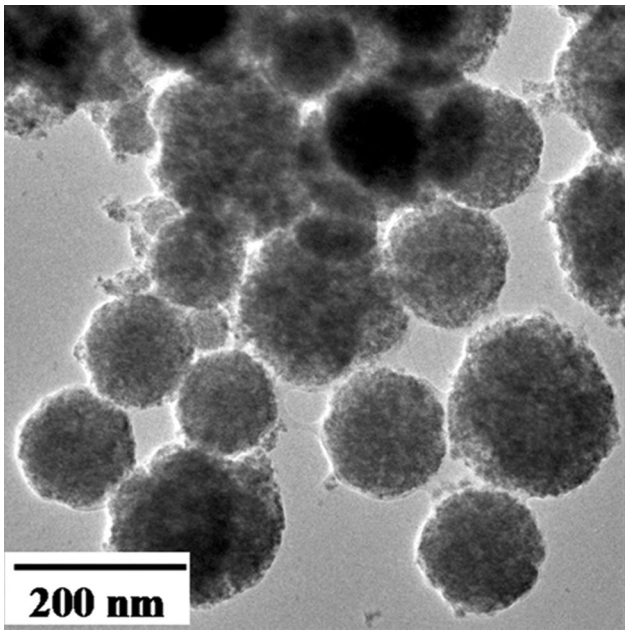

Fig. 2 TEM image of hybrid TiO_2/WO_3 precursor nanoparticles (Ti:W = 85:15) after acetone extraction several times

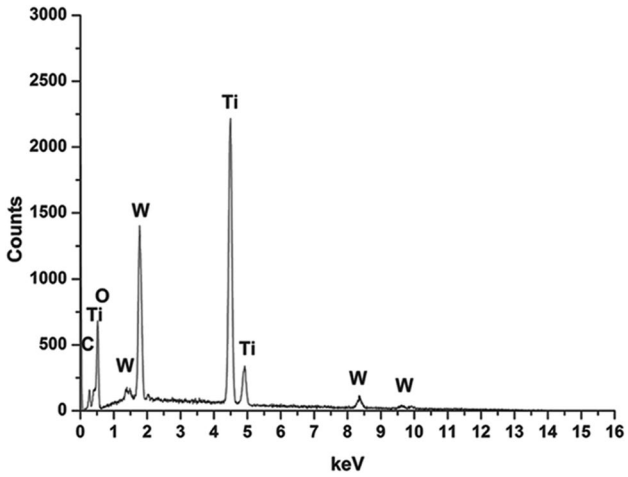

Fig. 3 EDS spectrum of hybrid TiO_2/WO_3 nanoparticles (Ti:W = 85:15) after calcination at 600 °C for 5 h

identified. The presence of C atom is probably attributed to residual C atom produced from the incomplete removal of PCL-*b*-PAA even after calcinations [48–50].

Figure 4 shows the typical XRD patterns of the TiO_2/WO_3 nanoparticles calcinated at various temperatures for 5 h. At 500 °C, the anatase peaks were mainly observed in the XRD patterns. At 700 °C, the rutile crystal peaks can be clearly identified, which reveals the temperature has a great impact on the transformation of crystal structure [51]. Also the peaks of orthorhombic WO_3 were observed at 700 °C, compared with the weak peaks at 500 °C and 600 °C, which may caused by the formation of amorphous WO_3. The anatase-to-rutile transformation temperature has been mostly reported from 600 to 900 °C for the initiation and finishing temperature, respectively [52].

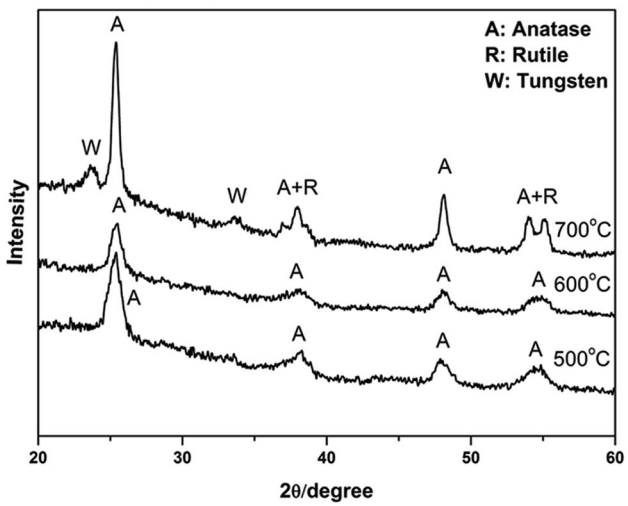

Fig. 4 The XRD patterns of hybrid TiO_2/WO_3 nanoparticles calcinated at 500 °C, 600 °C and 700 °C, respectively. A denotes anatase phase of TiO_2, R denotes rutile phase of TiO_2 and W denotes orthorhombic WO_3, respectively

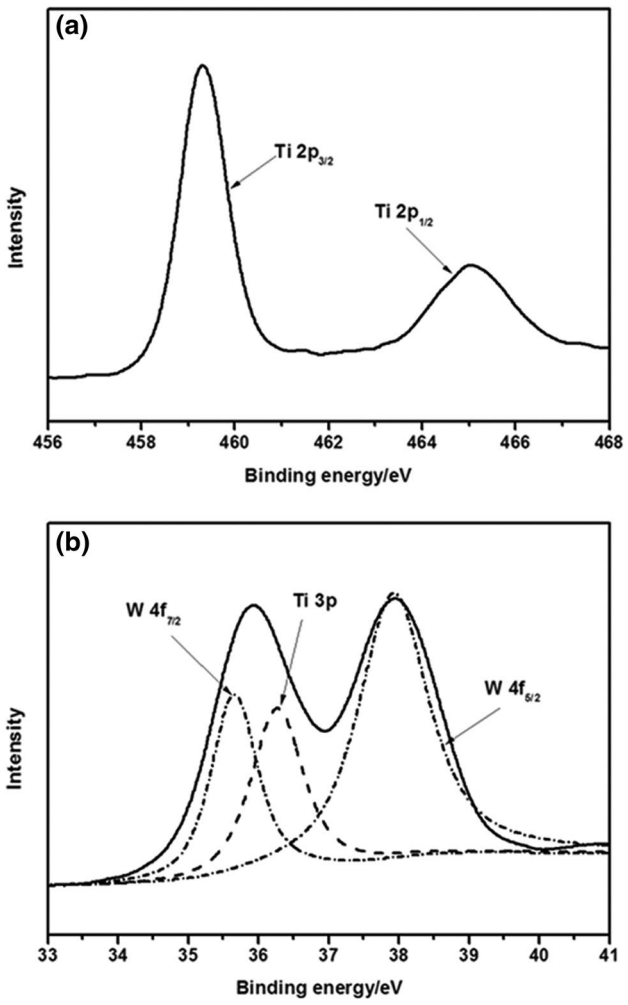

Fig. 5 XPS spectra of **a** Ti2p and **b** W4f and Ti3p of hybrid TiO_2/WO_3 nanoparticles (Ti:W = 85:15) after calcination at 600 °C. The solid lines are experimental spectra and the others are fitting ones

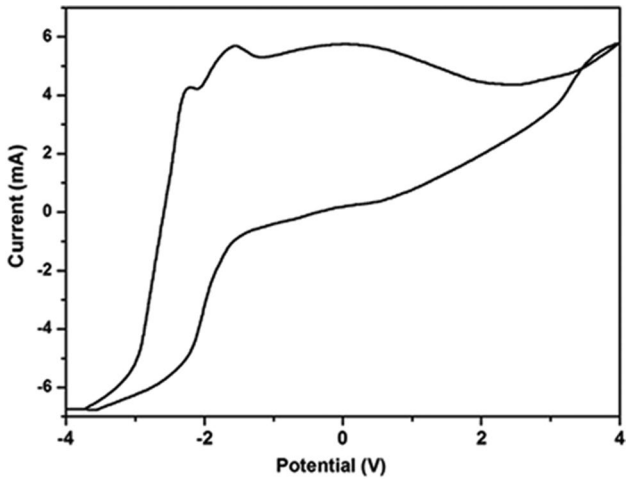

Fig. 6 Cyclic voltammetry curve of TiO_2/WO_3 (Ti:W = 85:15) spin-coated film after calcination at 600 °C

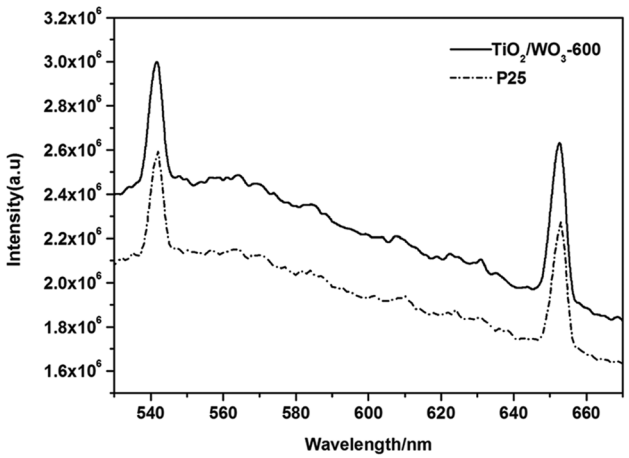

Fig. 7 PL spectra of TiO_2/WO_3-600 nanoparticles (Ti:W = 85:15, calcinated at 600 °C) and P25

XPS spectra of TiO_2/WO_3 nanoparticles displays two peaks at 459.1 eV and 464.8 eV (Fig. 5a) resulted by the spin orbit split of Ti2p, indicating the existence of the Ti–O bonds. Furthermore, the measured binding energy value is higher than the standard one is attribute to the transformation of Ti–O–Ti to Ti–O–W. Figure 5b showed the result of fitting peak separation curve. The peaks at 35.5 eV and 37.8 eV are attributed to the formation of W^{6+}, existing in the form of WO_3. While, the peak at 36.3 eV is corresponded to the Ti3p.

Figure 6 shows the cyclic voltammetry curve of TiO_2/WO_3 (Ti:W = 85:15) spin-coated film after calcinations at 600 °C. The closed circular curve demonstrates the coloring-fading process is reversible. There are two obvious anodic peak, corresponding to the different active points formed when Li^+ and H^+ are injected to the TiO_2/WO_3 film.

Photoluminescence emission spectra (PL) have been widely used to investigate the efficiency of charge trapping, immigration, transfer and to understand the fate of electron–hole pairs about the semiconductor particles [53]. Figure 7 shows the PL spectra of TiO_2/WO_3-600 (Ti:W = 85:15, calcinated at 600 °C) and P25. It can be seen that the PL intensity of TiO_2/WO_3 is much lower than that of P25. This indicated that WO_3 doping can effectively inhibit the recombination of photo-generated electrons and holes, in consequence the separation of light carriers inside TiO_2/WO_3 film is much better, and the absorption of light intensity degree is higher than that of P25, thus TiO_2/WO_3 might show stronger photocatalytic activity than P25.

Figure 8 displays the nitrogen adsorption–desorption isotherms and pore size distribution curve of TiO_2/WO_3-600 and P25. The TiO_2/WO_3-600 in this work exhibits a type IV isotherm and a type H_2 hysteresis loop [54]. The pore diameters of TiO_2/WO_3-600 and P25 are 8.5 and 9.9 nm,

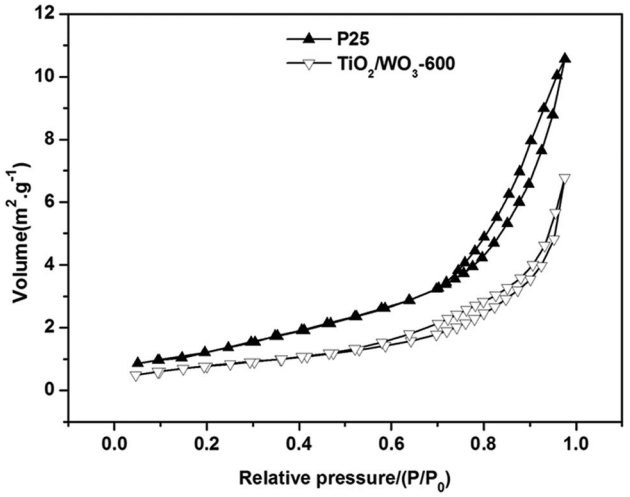

Fig. 8 BET curves of TiO_2/WO_3-600 nanoparticles (Ti:W = 85:15, calcinated at 600 °C) and P25

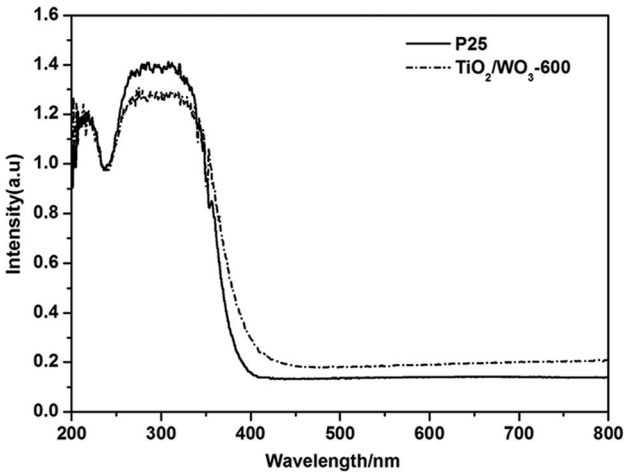

Fig. 9 UV–vis absorption spectra of TiO_2/WO_3-600 nanoparticles (Ti:W = 85:15, calcinated at 600 °C) and P25

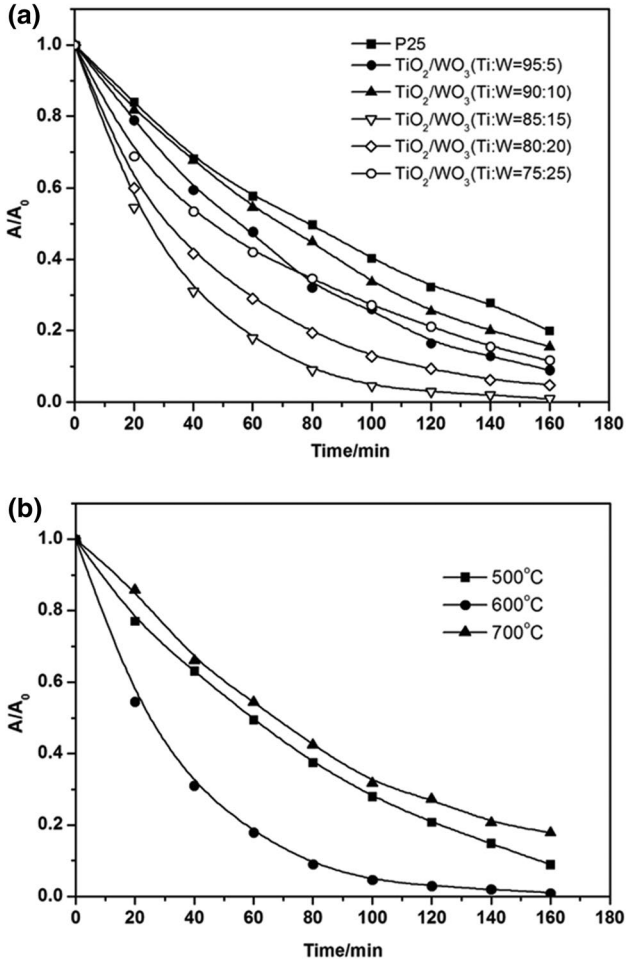

Fig. 10 Photodegradation curves of MB catalyzed by **a** TiO_2/WO_3-600 nanoparticles (Ti:W = 95:5, 90:10, 85:15, 80:20 and 75:25 respectively, calcinated at 600 °C) and P25; **b** TiO_2/WO_3 nanoparticles (Ti:W = 85:15) calcianted at 500 °C, 600 °C and 700 °C, respectively

respectively, indicating the formation of mesoporous structure. The smaller pore size reflects the inhibition of grain growth and aggregation of residual carbon due to polymer carbonization [54].

Figure 9 shows the UV–vis absorption spectra of TiO_2/WO_3-600 and P25. The enhanced absorption of TiO_2/WO_3-600 in the visible region can be attributed to the effect of WO_3 doping. The fundamental absorption band edge of P25 stopped at around 400 nm and did not show any visible light absorption, however, TiO_2/WO_3-600 showed an absorption extending beyond 400 nm. The difference in absorption characteristics of P25 and TiO_2/WO_3-600 proves that WO_3 was successfully doped into TiO_2 nanostructures. The visible light absorbance of TiO_2/WO_3-600 is attributed to the existence of tungsten species such as Ti–O–W bonds.

In order to investigate the photo catalytic behaviour of the as-synthesized TiO_2/WO_3 nanopartilces, the photodegradation of MB as a model pollutant was carried out. Firstly, the MB solution (10^{-3} g L^{-1}) was scanned at 200–800 nm. It found that the maximum intensity of the characteristic peak of MB at 665 nm decreased with increasing the irradiation time. So the variation of absorbance at 665 nm was used to show the photodegradation curve of MB. The photodegradation of MB by TiO_2/WO_3-600 with different doping ratios and P25 are shown in Fig. 10a. When the molar ratio of Ti/W is 85:15, the sample shows the best photocatalytic activity as MB can be completely photodegradation in shorter time. Besides all the doping act better photocatalytic activity compared with P25 under the same condition, this is due to the semiconductor of different width forbidden band compounded with each

other, urging the separation of electronic- hole, reducing electronic restructuring, widen the range of spectral response, further improve the photocatalytic efficiency [55]. Figure 10b shows the photodegradation curve of MB by TiO_2/WO_3-600 in doping ratio of Ti:W = 85:15 at different calcination temperature. It has been well understood that a higher activity can be achieved by improving many aspects of TiO_2-based photocatalysts, including surface area, crystallinity, absorption ability, non-mental doping and water dispersity [56, 57]. From a photocatalytic point of view, anatase is generally considered to be the more active phase due to its higher reduction potential and low re-combination rate of electron–hole pairs compared to rutile [58]. Therefore, the photocatalytic activity of TiO_2/WO_3-500 is better than TiO_2/WO_3-700. While, due to the special electronic states, the two crystal structures allow for a semiconductor–semiconductor junction [59]. TiO_2/WO_3-600 exhibits a higher photocatalytic activity than other photocatalysts. The TiO_2/WO_3-600 with the doping ratio of Ti:W = 85:15 can nearly completely degrade the MB solution (10^{-3} g L^{-1}) within 100 min.

4 Conclusions

Visible-light active hybrid TiO_2/WO_3 spherical nanoparticles were successfully fabricated via a sol–gel process using an amphiphilic PCL-*b*-PAA diblock copolymer as template followed by calcination. In comparison with commercial catalyst P25, the hybrid TiO_2/WO_3 exhibited better catalytic behaviour in the photodegradation of MB. Doping ratio of Ti:W and calcination temperature, in our case, have a great significance on the catalytic activity of such hybrid TiO_2/WO_3 nanoparticles. The best degradation activity was present by using the hybrid TiO_2/WO_3 nanoparticles with a doping ratio of Ti:W = 85:15 calcinated at 600 °C.

Acknowledgements The authors greatly appreciate the financial support from the National Natural Science Foundation of China (Nos. 50873093 and 21271156).

Compliance with ethical standards

Conflict of interest The authors declare that they have no conflict of interest.

References

1. McKeon-Fischer KD, Flagg DH, Freeman JW (2011) Poly(acrylic acid)/poly(vinyl alcohol) compositions coaxially electrospun with poly(ε-caprolactone) and multi-walled carbon nanotubes to create nanoactuating scaffolds. Polymer 52:4736–4743
2. Yao J, Wu H, Ruan Y, Guan J, Wang AN, Li HR (2011) "Reservoir" and "barrier" effects of ABC block copolymer micelle in hydroxyapatite mineralization control. Polymer 52:793–803
3. Zhu W, Li YL, Chen YM, Xi F (2012) Supramolecular hydrogels as a universal scaffold for stepwise delivering Dox and Dox/cisplatin loaded block copolymer micelles. Int J Pharm 437:11–19
4. Gou PF, Zhu WP, Xu N, Shen ZQ (2010) Synthesis and Self-assembly of well-defined cyclodextrin-centered amphiphilic A14B7 multimiktoarm star copolymers based on poly(ε-caprolactone) and poly(acrylic acid). J Polym Sci Polym Chem 48:2961–2974
5. Hameed N, Guo QP (2008) Nanostructure and hydrogen bonding in interpolyelectrolyte complexes of poly(ε-caprolactone)-*block*-poly(2-vinyl pyridine) and poly(acrylic acid). Polymer 49:5268–5275
6. Yuan C, Lu HC, Li QZ, Yang S, Zhao QL, Huang J, Wei LH, Ma Z (2012) Synthesis of well-defined amphiphilic polymethylene-*b*-poly(caprolactone)-*b*-poly(acrylic acid) triblock copolymer via a combination of polyhomologation, ring-opening polymerization, and atom transfer radical polymerization. J Polym Sci Polym Chem 50:2398–2405
7. Niu DC, Liu XH, Li YS, Ma Z, Dong WJ, Chang S, Zhao WR, Gu JL, Zhang SJ, Shi JL (2011) Fabrication of uniform, biocompatible and multifunctional PCL-*b*-PAA copolymer-based hybrid micelles for magnetic resonance imaging. J Mater Chem 21:13825–13831
8. Arnal P, Corriu RJP, Leclercq D, Mutin PH, Vioux A (1997) A solution chemistry study of nonhydrolytic sol–gel routes to titania. Chem Mater 9:694–698
9. Sugimoto T, Zhou X, Muramatsu A (2002) Synthesis of uniform anatase TiO_2 nanoparticles by gel–sol method. 1. Solution chemistry of $Ti(OH)_n^{(4-n)+}$ complexes. J Colloid Interface Sci 252:339–346
10. Sugimoto T, Zhou X (2002) Synthesis of uniform anatase TiO_2 nanoparticles by the gel–sol method 2. Adsorption of OH^- ions to $Ti(OH)_4$ Gel and TiO_2 particles. J Colloid Interface Sci 252:347–353
11. Trung T, Cho WJ, Ha CS (2003) Preparation of TiO_2 nanoparticles in glycerol-containing solutions. Mater Lett 57:2746–2750
12. Lim KT, Hwang HS, Ryoo W, Johnston KP (2004) Synthesis of TiO_2 nanoparticles utilizing hydrated reverse micelles in CO_2. Langmuir 20:2466–2471
13. Li Y, Lee NH, Hwang DS, Song JS, Lee EG, Kim SJ (2004) Synthesis and characterization of nano titania powder with high photoactivity for gas-phase photo-oxidation of benzene from $TiOCl_2$ aqueous solution at low temperatures. Langmuir 20:10838–10844
14. Kim KD, Kim SH, Kim HT (2005) Applying the Taguchi method to the optimization for the synthesis of TiO_2 nanoparticles by hydrolysis of TEOT in micelles. Colloids Surf A 254:99–105
15. Lafond V, Mutin PH, Vioux A (2004) Control of the texture of titania–silica mixed oxides prepared by nonhydrolytic sol–gel. Chem Mater 16:5380–5386
16. Tang J, Redl F, Zhu Y, Siegrist T, Brus L, Steigerwald ML (2005) An organometallic synthesis of TiO_2 nanoparticles. Nano Lett 5:543–548
17. Ruiz AM, Sakai G, Cornet A, Shimanoe K, Morante JR, Yamazoe N (2004) Microstructure control of thermally stable TiO_2 obtained by hydrothermal process for gas sensors. Sens Actuators, B 103:312–317
18. Kolen'ko YV, Churagulov BR, Kunst M, Mazerolles L, Colbeau-Justin C (2004) Photocatalytic properties of titania powders prepared by hydrothermal method. Appl Catal B 54:51–58
19. Nian JN, Teng H (2006) Hydrothermal synthesis of single-crystalline anatase TiO_2 nanorods with nanotubes as the precursor. J Phys Chem B 110:4193–4198

20. Das SK, Bhunia MK, Bhaumik A (2010) A self-assembled TiO_2 nanoparticles: mesoporosity, optical and catalytic properties. Dalton Trans 39:4382–4390
21. Dutta S, Patra AK, De S, Bhaumick A, Saha B (2012) Self-assembled TiO_2 nanospheres by using a biopolymer as a template and its optoelectronic application. ACS Appl Mater Interface 4:1560–1564
22. Kim CS, Moon BK, Park JH, Choi BC, Seo HJ (2003) Solvothermal synthesis of nanocrystalline TiO_2 in toluene with surfactant. J Cryst Growth 257:309–315
23. Li XL, Peng Q, Yi JX, Wang X, Li YD (2006) Near monodisperse TiO_2 nanoparticles and nanorods. Chem Eur J 12:2383–2391
24. Pradhan SK, Reucroft PJ, Yang F, Dozier A (2003) Growth of TiO_2 nanorods by metalorganic chemical vapor deposition. J Cryst Growth 256:83–88
25. Wu JM, Zhang TW, Zeng YW, Hayakawa S, Tsuru K, Osaka A (2005) Large-scale preparation of ordered titania nanorods with enhanced photocatalytic activity. Langmuir 21:6995–7002
26. Wu JM, Shih HC, Wu WT (2005) Electron field emission from single crystalline TiO_2 nanowires prepared by thermal evaporation. Chem Phys Lett 413:490–494
27. Mohammadi MR, Cordero-Cabrera MC, Fray DJ, Ghorbani M (2006) Preparation of high surface area titania (TiO_2) films and powders using particulate sol–gel route aided by polymeric fugitive agents. Sens Actuators, B 120:86–95
28. Sharma SK, Vishwas M, Narasimha Rao K, Mohan S, Reddy DS, Gowda KVA (2009) Structural and optical investigations of TiO_2 films deposited on transparent substrates by sol–gel technique. J Alloys Compd 471:244–247
29. Li X, Fu XN, Yang H (2011) Preparation and photocatalytic activity of eccentric Au–titania core–shell nanoparticles by block copolymer templates. Phys Chem Chem Phys 13:2809–2814
30. Rawolle M, Ruderer MA, Prams SM, Zhong Q, Magerl D, Perlich J, Roth SV, Lellig P, Gutmann JS, Mueller-Buschbaum P (2011) Nanostructuring of titania thin films by a combination of microfluidics and block-copolymer-based sol–gel templating. Small 7:884–891
31. Chen ZX, Wang WX, Takao Y, Matsubara T, Ren LM (2012) Characterization and fatigue damage of TiO_2 layer on spark-anodized titanium before and after hot water treatment. Appl Surf Sci 262:2–7
32. Wang XD, Xue XX, Li QY, Zhang M, Yang JJ (2012) Twice heat-treating to synthesize TiO_2/carbon composites with visible-lightphotocatalyticactivity. Mater Lett 88:79–81
33. Liu SH, Syu HR (2012) One-step fabrication of N-doped mesoporous TiO_2 nanoparticles by self-assembly for photocatalytic water splitting under visible light. Appl Energy 100:148–154
34. Cheng XW, Yu XJ, Xing ZP, Yang LS (2012) Enhanced visible light photocatalytic activity of mesoporous anatase TiO_2 codoped with nitrogen and chlorine. Int J Photoenergy 2012:593245
35. Pal U, Ghosh S, Chatterjee D (2012) Effect of sacrificial electron donors on hydrogen generation over visible light-irradiated nonmetal-doped TiO_2 photocatalysts. Transit Metal Chem 37:93–96
36. Tan YN, Wong CL, Mohamed AR (2012) Hydrothermal treatment of fluorinated titanium dioxide: photocatalytic degradation of phenol. Asia-Pac J Chem Eng 7:877–885
37. Kim JH, Nishimura F, Yonezawa S, Takashima M (2012) Enhanced dispersion stability and photocatalytic activity of TiO_2 particles fluorinated by fluorine gas. J Fluorine Chem 144:165–170
38. Chen YH, Xu TT, Li XY, Zhao QL, Huang J, Li YS, Wei LH, Ma Z (2013) The fabrication and characterization of TiO_2 nanospheres with high visible light photocatalytic activity by direct carbonization of block copolymer templates. New J Chem 37:1115–1121
39. Park JY, Lee JH, Choi DY, Hwang CH, Lee JW (2012) Influence of Fe doping on phase transformation and crystallite growth of electrospun TiO_2 nanofibers forphotocatalyticreaction. Mater Lett 88:156–159
40. Wang S, Lian JS, Zheng WT, Jiang Q (2012) Photocatalytic property of Fe doped anatase and rutile TiO_2 nanocrystal particles prepared by sol–gel technique. Appl Surf Sci 263:260–265
41. Nogawa T, Isobe T, Matsushita S, Nakajima A (2013) Ultrasonication effects on the visible-light photocatalytic activity of Au-modified TiO_2 powder. Mater Lett 90:79–82
42. Chauhan R, Kumar A, Chaudhary RP (2012) Structural and photocatalytic studies of Mn doped TiO_2 nanoparticles. Spectrochim Acta A 98:256–264
43. Carcel RA, Andronic L, Duta A (2012) Photocatalytic activity and stability of TiO_2 and WO_3 thin films. Mater Charact 70:68–73
44. Yang JK, Zhang XT, Liu H, Wang CH, Liu SP, Sun PP, Wang LL, Liu YC (2013) Heterostructured TiO_2/WO_3 porous microspheres: preparation, characterization and photocatalytic properties. Catal Today 201:195–202
45. Ren CJ, Qiu W, Chen YQ (2013) Physicochemical properties and photocatalytic activity of the TiO_2/SiO_2 prepared by precipitation method. Sep Purif Technol 107:264–272
46. Fateh R, Dillert R, Bahnemann D (2013) Preparation and characterization of transparent hydrophilic photocatalytic TiO_2/SiO_2 thin films on polycarbonate. Langmuir 29:3730–3739
47. Zhang LF, Eisenberg A (1995) Multiple morphologies of "Crew-Cut" aggregates of polystyrene-*b*-poly(acrylic acid) block copolymers. Science 268:1728–1731
48. Zori MH (2011) Synthesis of TiO_2 nanoparticles by microemulsion/heat treated method and photodegradation of methylene blue. J Inorg Organomet Polym Mater 21:81–90
49. Zurmühl C, Popescu R, Gerthsen D, Feldmann C (2011) Microemulsion-based synthesis of nanoscale TiO_2 hollow spheres. Solid State Sci 13:1505–1509
50. Das D, Shivhare A, Saha S, Ganguli AK (2012) Room temperature synthesis of mesoporous TiO_2 nanostructures with high photocatalytic efficiency. Mater Res Bull 47:3780–3785
51. Tripathi AK, Singh MK, Mathpal MC, Mishra SK, Agarwal A (2013) Study of structural transformation in TiO_2 nanoparticles and its optical properties. J Alloys Compd 549:114–120
52. Oskam G, Nellore A, Lee Penn R, Searson PC (2003) The growth kinetics of TiO_2 nanoparticles from titanium(IV) alkoxide at high water/titanium ratio. J Phys Chem B 107:1734–1738
53. Yamashita H, Ichihashi Y, Zhang SG, Matsumura Y, Souma Y, Tatsumi T, Anpo M (1997) Photocatalytic decomposition of NO at 275 K on titanium oxide catalysts anchored within zeolite cavities and framework. Appl Surf Sci 121:305–309
54. Kochuveedu ST, Jang YJ, Jang YH, Lee WJ, Cha M, Shin H, Yoon S, Lee S, Kim SO, Shin K, Steinhart M, Kim DH (2011) Visible-light active nanohybrid TiO_2/carbon photocatalysts with programmed morphology by direct carbonization of block copolymer templates. Green Chem 13:3397–3405
55. Ahmed MA, El-Katori EE, Gharni ZH (2013) Photocatalytic degradation of methylene blue dye using Fe_2O_3/TiO_2 nanoparticles prepared by sol–gel method. J Alloys Compd 553:19–29
56. Zhang Q, Joo JB, Lu ZD, Dahl M, Oliveira D, Ye MM, Yin YD (2011) Self-assembly and photocatalysis of mesoporous TiO_2 nanocrystal clusters. Nano Res 4:103–114
57. Ye MM, Zhang Q, Hu YX, Ge JP, Lu ZD, He L, Chen ZL, Yin YD (2010) Magnetically recoverable core–shell nanocomposites with enhanced photocatalytic activity. Chem Eur J 16:6243–6250
58. Fujishima A, Zhang XT, Tryk DA (2008) TiO_2 photocatalysis and related surface phenomena. Surf Sci Rep 63:515–582
59. Woan K, Pyrgiotakis G, Sigmund W (2009) Photocatalytic carbon-nanotube–TiO_2 composites. Adv Mater 21:2233–2239